Influence of Temperature and Grain Size on Austenite Stability in Medium Manganese Steels

YULONG ZHANG, LI WANG, KIP O. FINDLEY, and JOHN G. SPEER

With an aim to elucidate the influence of temperature and grain size on austenite stability, a commercial cold-rolled 7Mn steel was annealed at 893 K (620 °C) for times varying between 3 minutes and 96 hours to develop different grain sizes. The austenite fraction after 3 minutes was 34.7 vol pct, and at longer times was around 40 pct. An elongated microstructure was retained after shorter annealing times while other conditions exhibited equiaxed ferrite and austenite grains. All conditions exhibit similar temperature dependence of mechanical properties. With increasing test temperature, the yield and tensile strength decrease gradually, while the uniform and total elongation increase, followed by an abrupt drop in strength and ductility at 393 K (120 °C). The Olson–Cohen model was applied to fit the transformed austenite fractions for strained tensile samples, measured by means of XRD. The fit results indicate that the parameters α and β decrease with increasing test temperature, consistent with increased austenite stability. The 7Mn steels exhibit a distinct temperature dependence of the work hardening rate. Optimized austenite stability provides continuous work hardening in the temperature range of 298 K to 353 K (25 °C to 80 °C). The yield and tensile strengths have a strong dependence on grain size, although grain size variations have less effect on uniform and total elongation.

I. INTRODUCTION

RECENTLY, based on the pioneering work by Miller[1] and Merwin,[2,3] medium Mn steels have attracted considerable attention as a strong candidate for third generation advanced high strength steel (3G-AHSS) in the automotive industry because of their excellent mechanical properties.[4–12] Medium Mn steels typically contain 4~10 wt pct Mn with relatively low carbon, and have excellent products of strength and elongation over 30 GPa pct. For example, Luo et al.[13] achieved a tensile strength of 850 to 950 MPa combined with a ductility of 20 to 30 pct in a Fe-5Mn-0.2C steel. Shi et al.[14] reported that a Fe-7Mn-0.2C steel exhibited a high tensile strength of 1420 MPa with 31 pct total elongation. Cai et al.[15] developed a Fe-11Mn-0.18-C-3.8Al steel having a tensile strength of 1007 MPa and a total elongation of 65 pct. Cold-rolled and hot-dip galvanized trial coils with two compositions,

Fe-7Mn-0.14C and Fe-10Mn-0.15C-1.5Al, have been manufactured through batch annealing (BA) and continuous annealing (CA) mass production lines in 2014.[16] All of the coils exhibited tensile strengths of ~1000 MPa and ductilities of ~40 pct, including the 7Mn steel selected for the current investigation.

The properties of medium Mn steels are dependent on the alloying levels and intercritical annealing processing steps, which control the volume fraction and stability of retained austenite.[17,18] During intercritical annealing, C and Mn partition from ferrite into austenite, enhancing the stability of the austenite. Optimized stability results in austenite retention and a transformation-induced plasticity (TRIP) effect, providing superior mechanical properties. Therefore, many studies on the relationship between intercritical annealing and austenite volume fraction have been performed using a variety of compositions.[19–21] In principle, with increasing intercritical annealing temperature, the volume fraction of retained austenite gradually increases to a maximum and then drops sharply because a portion of austenite transforms to martensite during cooling, which can be predicted by the model derived by De Moor et al.[22]

Austenite stability is known to be a critical aspect related to the TRIP effect and the understanding of transformation behavior in medium Mn steels. Some factors influence the stability of the metastable retained austenite including chemical composition, grain size, mechanical stability (the yield strength of the austenite grains and dislocation structure in austenite), and temperature.[23–26] The Mn and C concentrations in austenite are mainly determined by intercritical

YULONG ZHANG is with the Research Institute, Baoshan Iron & Steel Co. Ltd., Shanghai, 201900, P.R. China, and also with the State Key Laboratory of Development and Application Technology of Automotive Steels (Baosteel), Shanghai, 201900, P.R. China, and also with the Advanced Steel Processing and Products Research Center, Colorado School of Mines, Golden, CO 80401. Contact e-mail: zhangyulong@baosteel.com LI WANG is with the Research Institute, Baoshan Iron & Steel Co. Ltd., and also with the State Key Laboratory of Development and Application Technology of Automotive Steels (Baosteel). KIP O. FINDLEY, and JOHN G. SPEER are with the Advanced Steel Processing and Products Research Center, Colorado School of Mines, Golden, CO 80401.

annealing temperature and holding time, which influence the phase fractions and compositions through a variety of thermodynamic and kinetic factors. A reduction in austenite grain size also suppresses the martensitic transformation and thus results in increased austenite stability. Lee et al.[27] predicted the austenite grain size as a function of the annealing temperature in a 0.3C-6Mn steel using DICTRA software. Analyses of the results suggested that the martensitic transformation start (Ms) temperature should substantially decrease as annealing temperature is decreased, when the temperature-dependent austenite grain size is considered. Lee et al.[28,29] reported that the retained austenite after intercritical annealing has a very low dislocation density and does not inherit the high dislocation density of the heavily deformed martensite of the cold-rolled starting condition, and therefore suggested that mechanical stabilization by dislocation debris does not contribute to the austenite stability in ultrafine-grained medium Mn steels. Furthermore, the yield strength of the austenite as determined by alloy concentration and grain size is another factor that may influence the austenite stability. Strengthening of austenite could lead to greater stability because more mechanical driving force is required for transformation to occur.

The influences of chemical composition, austenite volume fraction, and heat treatment on the mechanical properties and austenite stability have been intensively investigated in medium Mn steels.[1–10] However, deep understanding of grain size and temperature effects has not been achieved to date, which could offer potential for further improvement in the performance of these steels.

Therefore, the objective of this work was to study and understand the austenite stability associated with the strain-induced martensitic transformation in cold-rolled medium manganese steels, particularly the effect of test temperature and grain size on austenite stability and related transformation kinetic behavior.

II. EXPERIMENTAL PROCEDURE

The medium Mn steels used in this work were obtained from industrial trial production material. The chemical composition of this 7Mn steel is listed in Table I. The initial condition involved material that was hot-rolled, intercritically batch-annealed, and cold-rolled as follows: after steelmaking, the slabs with dimensions of $5000 \times 1250 \times 200$ mm were reheated to 1473 K (1200 °C) for 2 hours and hot-rolled with a finish rolling temperature of 1153 K (880 °C) and a coiling temperature of 873 K (600 °C). The thickness of the hot-rolled sheets was 2.8 mm. The intercritical batch annealing was conducted at 893 K (620 °C) for 12 hours. The hot-rolled sheets consisting of austenite and

ferrite had a tensile strength and total elongation of 889 MPa and 31.7 pct, respectively. They were pickled and then cold-rolled to a thickness of 1.4mm with a thickness reduction of 50 pct.

In order to obtain different grain sizes, the cold-rolled 7Mn steel sheets were heated to 893 K (620 °C) and held for 3 minutes, 12, 24, 48, or 96 hours. These steels are designated as 7Mn3, 7Mn12, 7Mn24, 7Mn48, and 7Mn96 in this paper, according to their respective annealing time. These annealing times are relevant to both continuous and batch annealing industrial processes.

Tensile specimens were machined along the rolling directions according to the ASTM-E8 standard with a gauge length of 50 mm × 12.5 mm. During testing at various temperature, the specimens were submerged into an oil tank, which was subsequently heated to the target temperature based on thermocouple measurements on the specimen. Then, tensile tests were conducted in the oil tank at a constant engineering strain rate of 0.001 s^{-1}. Specimens for X-ray diffraction (XRD) were taken from the uniformly strained region of tensile specimens close to the neck, ground with 600 grit SiC paper, and chemically polished with a 1:10:10 mixture of 48 pct hydrofluoric acid, 30 pct hydrogen peroxide, and de-ionized water at room temperature for 15 minutes. X-ray diffraction was conducted at room temperature with copper radiation using a Phillips X-pert diffractometer operating at 45 kV and 40 mA. The scan range of 2θ was 40 to 110 deg. Four γ peaks ({111}, {200}, {220}, and {311}) and four α peaks ({110}, {200}, {211}, and {220}) were used to estimate the austenite volume fraction. Scanning electron microscopy (SEM) was performed using a JEOL 7000F FESEM. Specimens for electron backscatter diffraction (EBSD) analysis were polished to 1 μm with diamond paste and then with colloidal silica for 4 hours on a vibratory polisher (Vibromet 2). The EBSD scans were performed using an FEI Helios NanoLab 600i dual-beam microscope operating at an accelerating voltage of 20 kV with a scanning step size of 30 nm. EDAX-TSL OIM Data Collection and TSL OIM analysis 7 software were used for data acquisition and analysis.

III. RESULTS

A. Microstructural Characterization and Mechanical Properties

Figure 1 shows the Image Quality (IQ) plus Phase images for the five 7Mn conditions. As shown in Figure 1, the microstructural constituents in the 7Mn steels are primarily ferrite (F) and retained austenite (A). In addition to the difference in austenite fractions between the 7Mn3 and the other four conditions, metallography reveals some other changes in

Table I. Chemical Composition of Experimental Steel, in Weight Percent

Steel	C	Mn	Si	Al	N	S	P
7Mn	0.14	7.14	0.23	0.056	0.012	0.002	0.007

microstructure with annealing time. An elongated morphology shown in Figure 1(a) for the 7Mn3 condition is apparent compared to other conditions, implying that in the short annealing time, martensite boundaries constrained the growth of ferrite and austenite and recrystallization of ferrite may be incomplete. The darker contrast associated with reduced image quality at short annealing time is also consistent with this interpretation. The microstructures for annealing times longer than 12 hours are shown in Figures 1(b) through (e) and display equiaxed ferrite and austenite, suggesting that some movement of the austenite and ferrite grain boundaries has occurred after a longer period of annealing.

The EBSD images in Figure 1 also show that the grain size of ferrite and austenite increase systematically with annealing time. Table II summarizes the average grain sizes calculated using the weighted average with respect to area fraction for all five steels. The grain growth behavior with annealing time can be expressed with the following relationship:

$$d^2 - d_0^2 = st,$$

where d is the grain size at time t and s is a constant of proportionality.[30] The experimental data, fit using the above equation, are shown in Figure 2. The slope for ferrite is much greater than that for austenite, implying a greater tendency for the ferrite grains to grow in this microstructure over the annealing times of interest.

Table II shows the austenite volume fraction at room temperature as a function of annealing time for the 7Mn steel at 893 K (620 °C). Austenite volume fractions were obtained using both XRD and EBSD. As shown in Table II, the XRD and EBSD measured fractions of austenite in the 7Mn3 condition, 34.7 and 24.9 vol pct, are the lowest of the five 7Mn conditions because of the shortest annealing time of 3 minutes, where little Mn partitioning is likely. Most of the austenite stabilization in this condition is presumably associated with the Mn partitioning that occurs during intercritical batch annealing prior to cold rolling. The observed austenite amounts in the other four steels are similar and do not exhibit a systematically increasing or decreasing trend with prolonged annealing time. The deviation between the EBSD measured value and actual austenite fraction in the samples can be influenced by the small scan area or by a very small feature size. The austenite fraction of 35.1 vol pct as measured by XRD in the 7Mn96 steel is slightly less than the other three conditions. Application of the model proposed by De Moor et al.[22] predicts 41 vol pct austenite for the 7.1Mn steels annealed at 893 K (620 °C). XRD and neutron diffraction measurements made on a similar 0.1 C-7.1Mn steel annealed at 898 K for 168 hours exhibited 39 and 45.2 vol pct austenite,
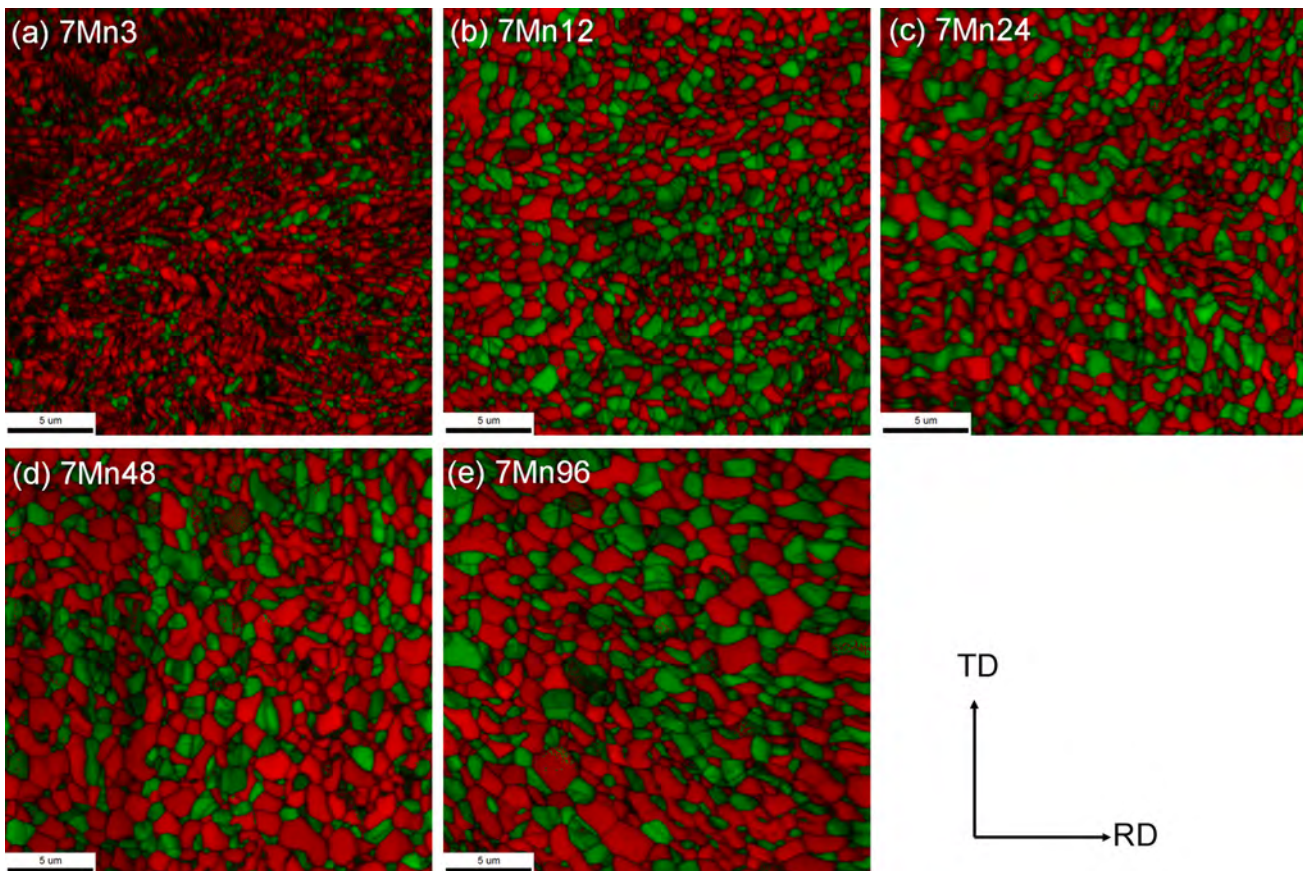

Fig. 1—EBSD Image Quality (IQ) plus Phase maps for 7Mn steel annealed at 893 K (620 °C) for different times (ferrite in red, austenite in green).

Table II. Austenite Volume Fraction, Tensile Properties, and Grain Size at Room Temperature

| Steel	Annealing Temp./Time	YS (MPa)	UTS (MPa)	Total El (Pct)	Austenite Volume Fraction (Pct)		Average Grain Size (μm)	
					XRD	EBSD	Ferrite	Austenite
7Mn3	893 K (620 °C)/3 min	1046	1054	33.2	34.7	24.9	0.93	0.31
7Mn12	893 K (620 °C)/12 h	801	1074	39.7	38.4	39.7	1.19	0.69
7Mn24	893 K (620 °C)/24 h	720	1016	40.3	40.0	35.1	1.72	0.76
7Mn48	893 K (620 °C)/48 h	697	1059	38.9	38.8	32.1	2.47	0.67
7Mn96	893 K (620 °C)/96 h	630	1023	39.6	35.1	36.6	2.54	0.94
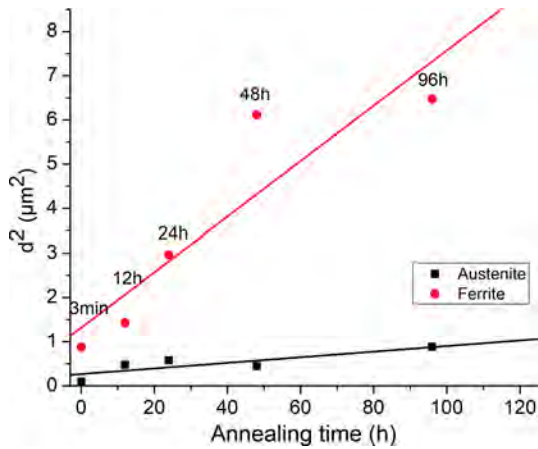
Fig. 2—Grain size squared as a function of annealing time at 893 K (620 °C) for the 7Mn steels, including experimental and fit results.

respectively and no martensite was found.[18] Therefore, the difference in the experimentally measured amount of austenite as a function of annealing time between 12 and 96 hours is within the range of uncertainty in the XRD measurement, and the retained austenite fractions in the 7Mn12, 7Mn24, 7Mn48, and 7Mn96 steels are similar at about 40 vol pct.

Table II also presents a summary of the room temperature mechanical properties for the five conditions, manifesting excellent products of strength and ductility of around 40 GPa pct. The yield strength is noted to decrease with annealing time, presumably due to recovery and recrystallization in the very early stage of annealing, as well as ferrite grain growth in the later stage. Tensile strength remains almost unchanged with annealing time within the experimental uncertainty. The total elongation for the 7Mn3 condition is 33.2 pct while that for the other four conditions is around 40 pct, indicating that incomplete recrystallization resulted in lower ductility.

B. Temperature-Dependent Tensile Properties

Figure 3 shows the quasi-static ($\dot{\varepsilon} = 10^{-3} s^{-1}$) engineering stress–strain curves for the 7Mn steels over a temperature range of 193 K to 393 K (−80 °C to 120 °C). As can be seen from Figure 3a, the 7Mn3 steel exhibits little or no work hardening at temperatures higher than 333 K (60 °C). The curve at 333 K (60 °C)

is almost totally 'flat' indicating that Lüders band propagation may occur up to large strains at high temperature. When the test temperature continues to increase, the elongation drops from about 40 to 10 pct at 353 K (80 °C), and little transformation is noted. The severely reduced ductility and the observation of strain lines on the sample surface for the 353 K (80 °C) condition suggested that deformation is localized because of the absence of strain-induced transformation and associated work hardening. Therefore, the results imply that increased ductility is achieved only if the Lüders band can propagate along the whole sample with the support of transformation. All the other stress–strain curves in Figures 3(b) through (e) display discontinuous yielding followed by work hardening, resulting in high elongation values. Most of the stress–strain curves exhibit serrations in the strain-hardening regime, likely associated with dynamic strain aging and/or strain-induced transformation from austenite to martensite.

Figure 4 compares the tensile properties for the 7Mn steels annealed for different times, including yield strength (YS), tensile strength (TS), total elongation (EL), and product of strength and ductility (EL*TS). The results are average values from duplicate tensile tests in all conditions.

The five conditions display a similar influence of test temperature on tensile properties. The yield strengths go down monotonically with increasing temperature, and the tensile strengths exhibit an even greater downward trend with increasing temperature. The yield strength for the 7Mn3 steel is much higher than the other four steels by about 400 MPa. The tensile strength of the 7Mn3 steel is also higher than the other four steels by about 200 MPa at test temperatures lower than 333 K (60 °C). At temperatures above ambient, the tensile strength for the 7Mn3 steel remains essentially unchanged at around 1050 MPa, while the other four steels tend to drop substantially with increased temperature, as shown in Figure 4.

The ductility results for the 7Mn steels highlight two significant trends. First, a pronounced maximum in total elongation is observed with changes in test temperature, followed by a significant decrease. Another important observation is the limited post-uniform elongation for all conditions, which results in total elongation values close to the uniform elongation. The maximum elongation values for the 7Mn3 steel are at about 313 K
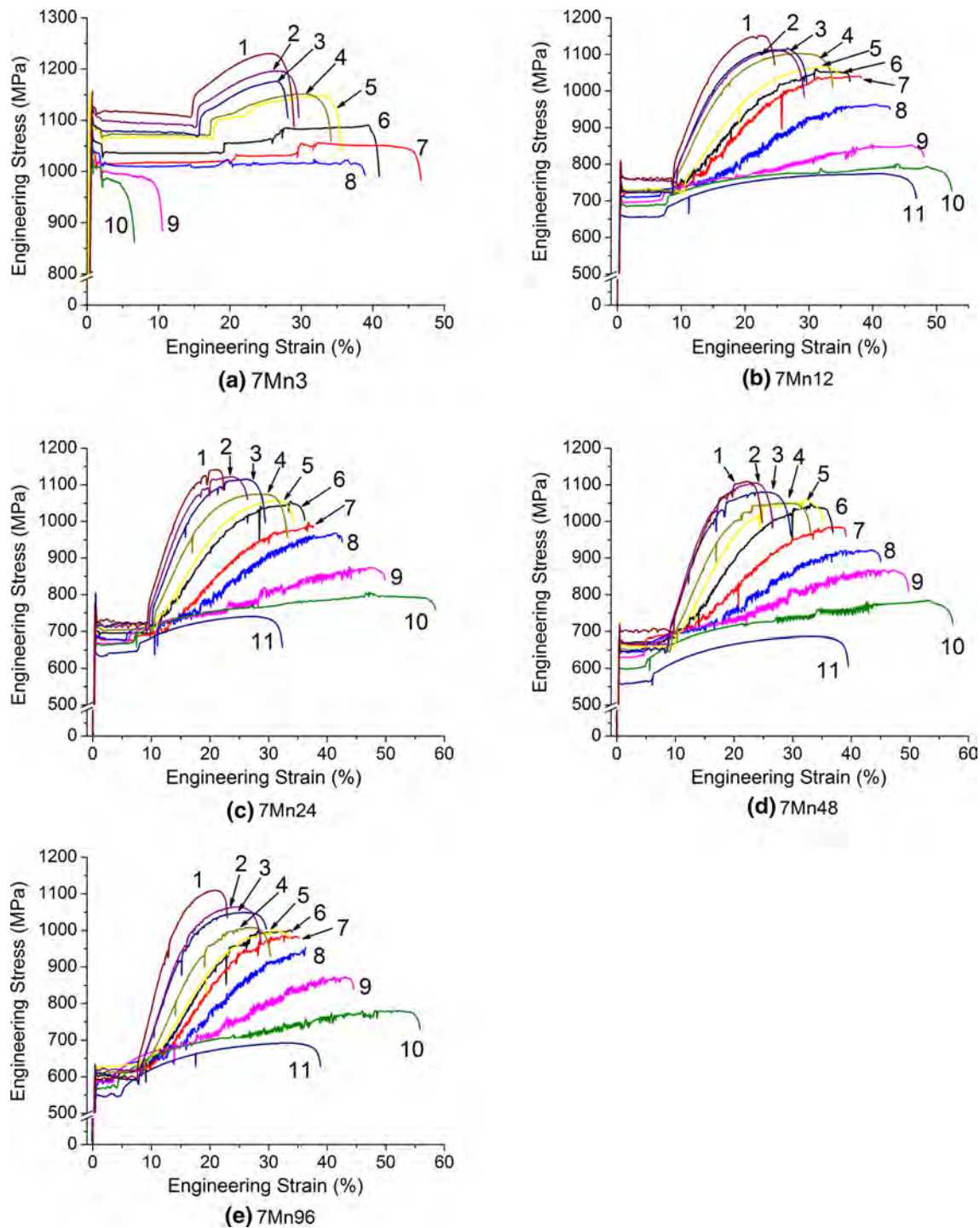
Fig. 3—Engineering stress–strain curves for 7Mn steels at various temperatures. Samples were tested at a constant engineering strain rate of 0.001 s^{-1}. The label in figures and related test temperatures were as follows: 1. 193 K (−80 °C), 2. 213 K (−60 °C), 3. 233 K (−40 °C), 4. 253 K (−20 °C), 5. 273 K (0 °C), 6. 298 K (25 °C), 7. 313 K (40 °C), 8. 333 K (60 °C), 9. 353 K (80 °C), 10. 373 K (100 °C), 11. 393 K (120 °C).

(40 °C), while the other steels exhibit maximum elongation at a temperature of about 373 K (100 °C).

The combination of strength and ductility is also highlighted in the TS*EL product shown in Figure 4(d), as a measure of performance during plastic deformation. Increasing test temperature results in a peak in the plot for all five steels. The peak temperatures appear at

313 K and 373 K (40 °C and 100 °C) for 7Mn3 and the other four steels, respectively.

Figure 5 presents the normalized fraction of austenite transformed (to martensite) after tensile testing as a function of test temperature for all five 7Mn steels. The normalized austenite fraction is defined as the value of the transformed fraction divided by the initial value. The five
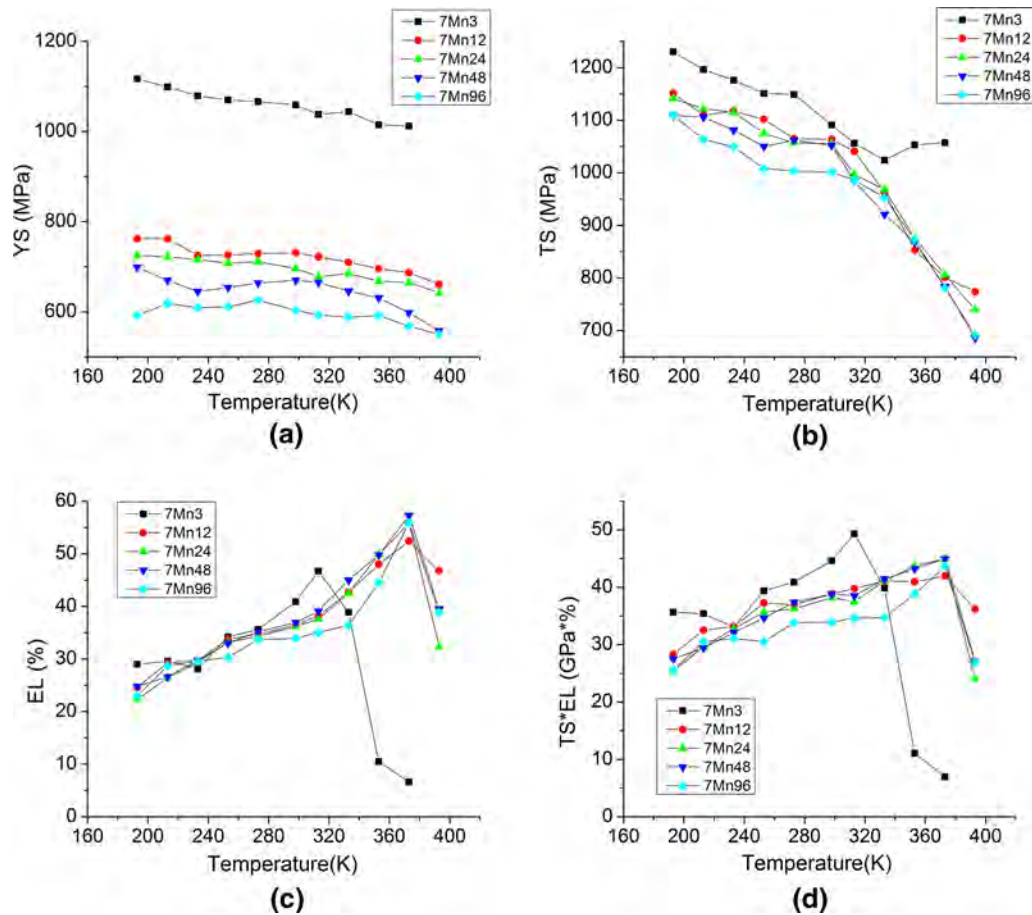
Fig. 4—Tensile properties as a function of test temperature for the 7Mn steels. (*a*) variation of YS with temperature, (*b*) variation of TS with temperature, (*c*) variation of EL with temperature, and (*d*) variation of TS*EL with temperature.

steels exhibit the same trend. With increasing test temperature, more austenite remains untransformed. For the 7Mn3 steel, all of the austenite transformed to martensite when the temperature was below about 273 K (0 °C). This critical temperature shifts to about 298 K (25 °C) for the 7Mn12, 7Mn24, and 7Mn48 steels and to about 333 K (60 °C) for the 7Mn96 steel. As expected, the austenite is more stable at higher test temperatures.

Above 273 K (0 °C), the amount of untransformed austenite varies with annealing time. The 7Mn3 steel always shows the lowest amount of transformation, and the 7Mn96 steel exhibits the greatest. The shorter the annealing time, the more the austenite remains untransformed after tensile testing. 36.9 and 27 vol pct austenite, respectively, were observed at room temperature for 7Mn12 and 7Mn96 steels after testing at 393 K (120 °C). Only about 4 pct of the austenite present in the 7Mn12 steel transformed at 393 K (120 °C), whereas 23 pct of the austenite in the 7Mn96 steel transformed at 393 K (120 °C). That is, the longer annealing time was associated with the lowest austenite stability. At 393 K (120 °C), the 7Mn12 steel exhibits excellent ductility (over 40 pct elongation) although only a little transformation takes place, which implies that at elevated temperature the austenite is very stable and has less contribution to work hardening. Therefore, high ductility
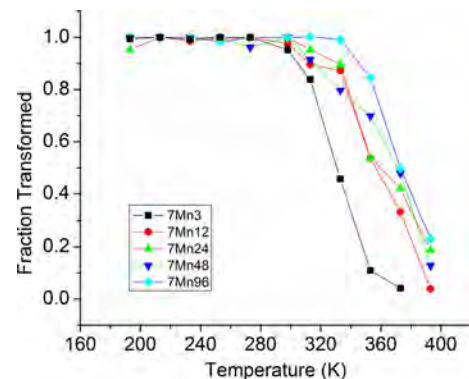

Fig. 5—Fraction of austenite transformed (to martensite) after tensile testing as a function of test temperature for 7Mn steels.

is achieved not through work hardening associated with TRIP in this steel, but *via* other mechanisms such as slip and deformation twinning in the austenite. While longer annealing times may increase austenite stability *via* increased Mn partitioning, in this study extensive Mn partitioning was promoted during the intercritical batch annealing process prior to cold rolling and final annealing, and the effect of austenite grain growth on austenite stability at longer annealing time appears to dominate.
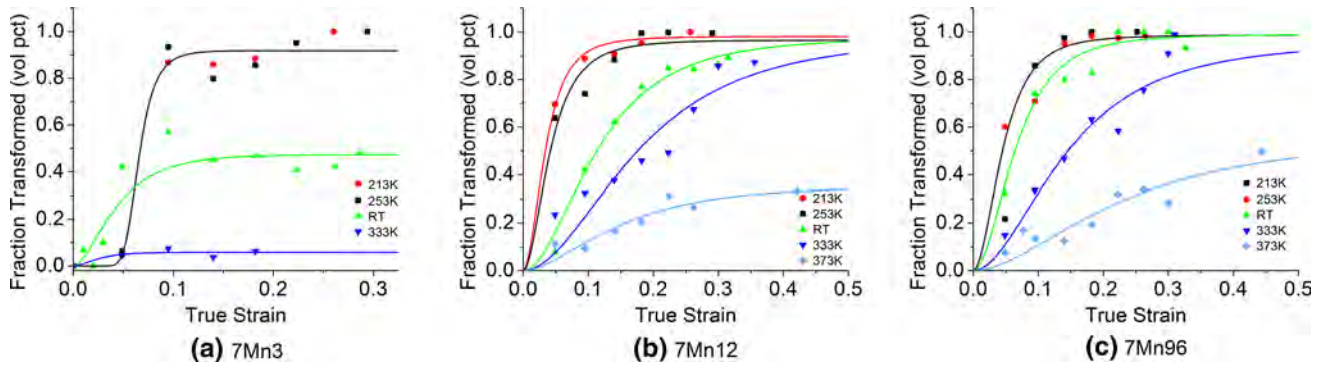
Fig. 6—Austenite transformation kinetics for five 7Mn steels based on the OC model.

Table III. Olson–Cohen Model Parameters for Austenite Transformation in Various Steels

Temp.		α	β	n		α	β	n		α	β	n
−60	7Mn3	60.83	2.5	75.71	7Mn12	16	3.94	2	7Mn24	21.46	4.42	2
−20		60.83	2.5	75.71		14.23	3.94	2		16.47	3.23	2
RT		29.53	0.64	2		4.87	3.85	2		10.23	2.29	2
60		50.96	0.06	2		3.18	3.77	2		6.34	2	2
100						8.12	0.43	2		9.13	0.52	2
−60	7Mn48	21.67	4.22	2	7Mn96	11.36	4.33	2	7.1Mn*	6.37	0.67	2.67
−20		21.67	4.22	2		11.36	4.33	2	7.1Mn**	5.75	2.5	3
RT		9.69	2.59	2		7.65	4.61	2	7.1Mn†	18.6	1.86	2
60		7.95	1.47	2		4.34	3.16	2	7.1Mn‡	49.5	1.8	2
100		6.95	0.73	2		4.83	0.769	2	304 SS§	3.53	0.52	4.5

*,**,†,‡7.1Mn steels annealed at 848, 873, 898, and 923 K for 168 hours, respectively,[18] were tested at room temperature.
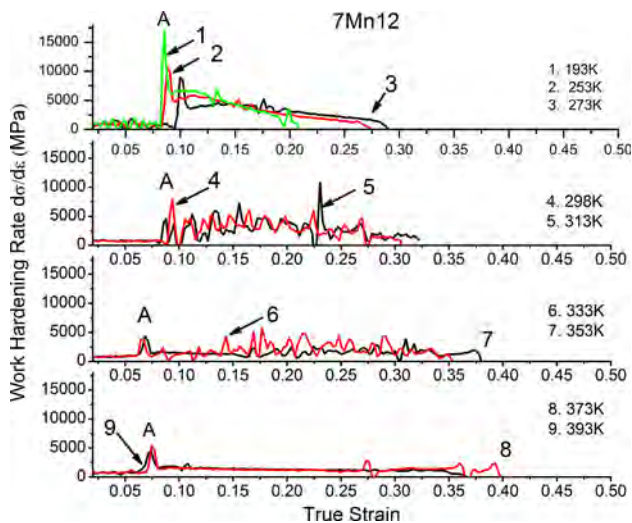§In Ref. [31].

Fig. 7—Temperature dependence of work hardening rate in the 7Mn12 steel.

C. Transformation Kinetics

Olson and Cohen (OC) proposed a model to describe strain-induced transformation assuming that shear band intersections act as martensitic nuclei.[31] The strain-induced fraction transformed is expressed as follows:

$$f_{\alpha'} = 1 - \exp\{-\beta[1 - \exp(-\alpha\varepsilon)]^n\},$$

where α is related to the rate of shear band formation, and thereby the stacking fault energy of the austenite and the strain rate, while β is related to the probability of martensite nucleation at a shear band intersection, which is dependent on the chemical driving force for austenite to martensite transformation and the necessary strain energy for transformation. The parameter n is a geometric constant relating the orientation of shear bands and the probability of shear band intersection.

Figure 6 shows the austenite fraction transformed as a function of true strain along with curve fits based on the OC model for the five 7Mn steels. Austenite fractions were measured up to the uniform elongation. Some of the steel conditions did not show appreciable differences within the range of experimental error, like the 253 K (−20 °C) and 213 K (−60 °C) results for the 7Mn3, 7Mn48, and 7Mn96 steels, which are thus combined using one fitted curve.

Table III summarizes the results for fitting of the OC model to the experimental data along with some values found in literature for a 7.1Mn steel and a 304 stainless steel. A geometric constant $n = 2$ is found to give the best overall agreement except for the 253 K (−20 °C) and 213 K (−60 °C) conditions in the 7Mn3 steel. The value of 2 represents a random distribution of shear band
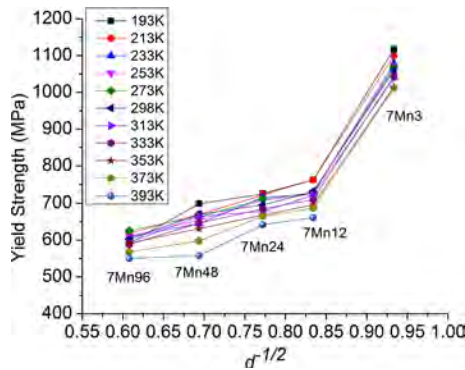
Fig. 8—Yield strength *vs* inverse of the square root of fitted grain size ($d^{-1/2}$) at various test temperatures.

orientations; *n* values greater than 2 correspond to some degree of parallelism of the shear bands, slowing the transformation rate. The derived value of *n* for the 7Mn3 steels at 253 K (−20 °C) and 213 K (−60 °C) is much greater than 2, implying a different transformation behavior in contrast to other steels, which will be discussed later. The fit results show that the temperature-dependent parameters α and β decrease with increasing ambient temperature, indicating increased austenite stability.

IV. DISCUSSION

A. *Recrystallization*

In general, the annealing temperature in a typical continuous annealing process is usually higher than that of batch-type annealing, in order to complete the recrystallization of the cold-rolled structure following rapid heating and short holding times. The 7Mn3 steel in this study was annealed at relatively low temperature and very short annealing time. This steel can be produced through a continuous annealing line while the other four steels would correspond to batch-annealed products. Some of the experimental results suggest that ferrite recrystallization in the 7Mn3 steel is not completed, because the elongated microstructure resembles a deformed structure, and there is a large difference in the mechanical properties between the transverse and rolling directions.[16] In addition, the elongated morphology observed in Figure 1 suggests that the formation of both austenite and ferrite is promoted by the prior martensite structure at an early stage of annealing, which contributes to the unusual properties in the 7Mn3 steel annealed for a very short time.

B. *Work Hardening Behavior*

Figure 7 displays the temperature dependence of the work hardening rate calculated from the true stress–strain curves in the 7Mn12 steel. Similar general behaviors were observed for the other annealing conditions. Overall, the contributions to work hardening arise from strain-induced transformation of austenite to martensite, dynamic strain aging (DSA), dislocation

multiplication in the ferrite and austenite, and possibly deformation twinning in the austenite.

In the strain range of 5 to 10 pct, the maximum work hardening rate, marked "A," corresponds to the end of the Lüders strain, and the position of the peak A increases to higher strains with decreasing test temperature. In the later part of curves, the shape is quite different. At temperatures over 373 K (100 °C), the curves are almost "flat," while they are more serrated in the range of 298 K to 353 K (25 °C to 80 °C). When the temperature is lower than 273 K (0 °C), the work hardening rate decreases gradually with increased strain. In combination with the transformation kinetics shown in Figure 6, the work hardening behavior is apparently related to austenite stability and the associated amount of phase transformation from austenite to martensite. In general, austenite stability decreases with decreasing test temperature. Reduced austenite stability at 273 K (0 °C) results in a large amount of transformation at the end of the Lüders strain, leading to a greater peak in the hardening rate at point "A." The "flat" behavior at temperatures over 373 K (100 °C) reflects enhanced austenite stability and indicates that transformation is not appreciable in the later part of curves.

Two types of propagative bands, Lüders bands and Portevin—Le Châtelier (PLC) bands, are typical forms of plastic instability in metal deformation. Lüders bands, commonly caused by static strain aging (SSA), usually form immediately after the yield point drop and are characterized by regions of localized strain as well as a corresponding stress plateau. Lüders strain in medium Mn steels has been observed and investigated in many studies.[32,33] The early instability as shown by samples 9 and 10 in Figure 3(a) shows that Lüders band propagation does not contribute to macroscopic work hardening. The PLC bands refer to a variety of irregular inhomogeneous deformation mechanisms, which are usually associated with dynamic strain aging effects. As shown in Figure 3, the smooth curves at relatively low test temperature imply that strain-induced transformation dominates the deformation behavior. Irregular stress serrations are observed at somewhat higher temperature, indicating DSA.[34,35] It is worth noting that serrations gradually become regular at a temperature close to 373 K (100 °C), perhaps indicating another mechanism that needs further investigation.

C. *Grain Size Effects*

The yield and tensile strength have a strong dependence on grain size, while the grain size did not suggest a systematic effect on total elongation based on the results in Figure 4. Figure 8 presents the relationship between yield strength and the inverse of the square root of grain size of ferrite ($d^{-1/2}$) at different test temperatures. The fitted grain sizes from Figure 2 were used in this plot instead of experimental ones from EBSD. As can be seen from Figure 8, for the 7Mn steels with annealing times longer than 12 hours, the linear dependence of yield strength on $d^{-1/2}$ suggests an apparent Hall–Petch-type relation. However, the 7Mn3 steel exhibits a yield strength much higher than the linearly
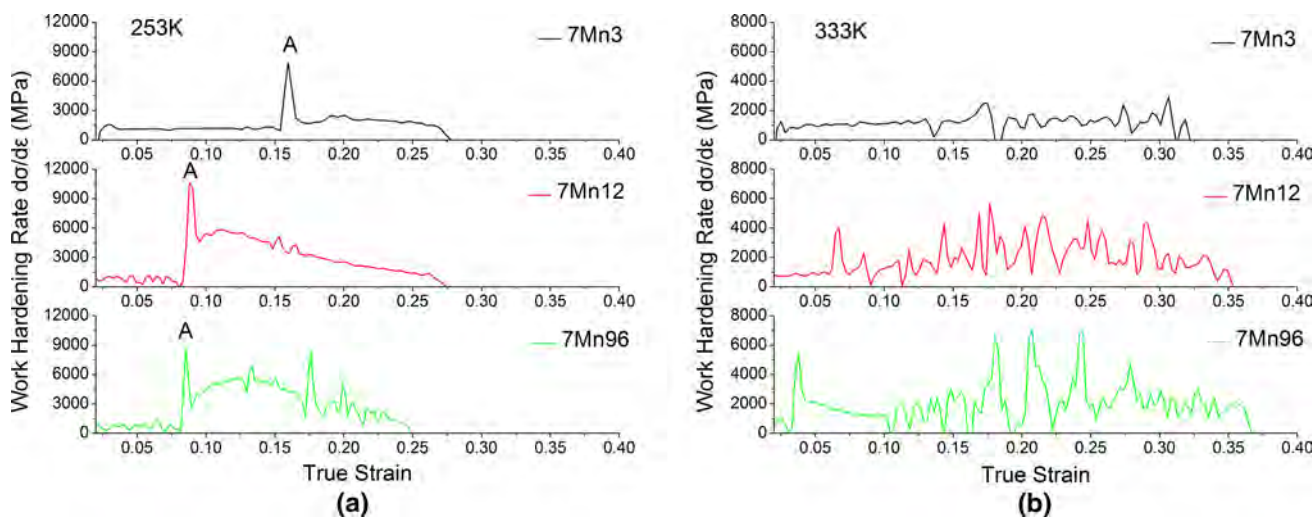
Fig. 9—Work hardening behavior of the 7Mn3, 7Mn12, and 7Mn96 steels at 253 K (−20 °C, left) and 333 K (60 °C, right).

extrapolated values, which presumably results from incomplete recrystallization.

The ductility for the five steels shown in Figure 4 does not exhibit a systematic trend with grain size. At a given test temperature, the differences in uniform and total elongation for the 7Mn steels are not appreciable except for the 7Mn3 steel, suggesting that the variation of austenite stability resulting from grain size variations in the experimental range is not enough to bring about a substantial change in ductility.

Figure 9 shows the end of discontinuous yielding (point "A") and the work hardening rate in the 7Mn3, 7Mn12, and 7Mn96 steels at 253 K (−20 °C) and 333 K (60 °C), respectively, illustrating the different work hardening behavior associated with austenite stability in steels having different grain sizes. At 253 K (−20 °C), the 7Mn3 steel displays a smooth work hardening curve after the peak A and the work hardening value is around 2000 MPa. The 7Mn12 and 7Mn96 steels have a similar curve shape except for serrations in the later part of the curve for the 7Mn96 steel, and the onset of continuous flow at lower strain. At 333 K (60 °C), the work hardening rate is around 1000 MPa for the 7Mn3 condition and small serrations are evident. In contrast, the results for the 7Mn12 and 7Mn96 steels exhibit more substantial serrations, possibly indicative of differences in DSA or TRIP behavior. It is noted that the austenite in the 7Mn3 steel with average grain size of 0.30 μm has the greatest stability and reduced work hardening. In the 7Mn12 and 7Mn96 steels, work hardening is greater, presumably because of the larger grain size.

V. CONCLUSIONS

The influence of grain size and temperature on austenite stability has been investigated in a 7Mn steel processed with variations in the intercritical annealing time. The following important conclusions were drawn:

- The 7Mn steels annealed for five different times at 893 K (620 °C) exhibit different grain sizes. The

austenite fraction in the 7Mn3 steel was 34.7 vol pct, and in the other steels was around 40 pct. The 7Mn3 condition retains an elongated microstructure while the other four steels show equiaxed ferrite and austenite grains.

- All five steels exhibit a similar general temperature dependence of mechanical properties. With increasing test temperature, the yield and tensile strength decrease gradually, and the uniform and total elongation increase, followed by an abrupt decrease at 393 K (120 °C).

- The Olson–Cohen model was applied to fit the transformed austenite fractions for prestrained samples, measured by means of XRD. The fit results show that the parameters α and β decrease with increasing test temperature, indicating increased austenite stability.

- The 7Mn steels exhibit a distinct temperature dependence of the work hardening rate. Optimized austenite stability provides continuous work hardening in the temperature range of 298 K to 353 K (25 °C to 80 °C).

- The yield and tensile strength have a strong dependence on grain size, however, it seems that grain sizes have little effect on values of uniform and total elongation in these conditions.

REFERENCES

1. R.L. Miller: *Metall. Trans.*, 1978, vol. 3, pp. 905–12.
2. M. J. Merwin: *Proc. of Mater. Sci. and Technol. 2007*, Detroit, 2007.
3. M.J. Merwin: *Iron & Steel Technology*, 2008, vol. 5, pp. 66–84.
4. H. J. Jun, O. Yakubovsky and N. Fonstein: *HMnS 2011 conf. Proc.*, Seoul, 2011.
5. Q. Han, Y. Zhang, and L. Wang: *Metall. Mater. Trans. A*, 2015, vol. 46A, pp. 1917–26.
6. Z.H. Cai, H. Ding, Z.Y. Tang, and R.D.K. Misra: *Mater. Sci. Eng. A*, 2016, vol. 676, pp. 289–93.
7. S. Lee, K. Lee, and B.C. De Cooman: *Mater. Sci. Forum*, 2010, vols. 654–656, pp. 286–89.
8. S. Lee, S. Lee, S.S. Kumar, K. Lee, and B.C. De Cooman: *Metall. Mater. Trans. A*, 2011, vol. 42A, pp. 3638–51.

9. D.K. Matlock, J.G. Speer, E. De Moor, and P.J. Gibbs: *Jestech*, 2012, vol. 15, pp. 1–12.
10. M.I. Latypov, S. Shin, B.C. De Cooman, and H.S. Kim: *Acta Mater.*, 2016, vol. 108, pp. 219–28.
11. A. Arlazarov, M. Gouné, O. Bouaziz, A. Hazotte, and F. Kegel: *Mater. Sci. Forum*, 2012, vols. 706–709, pp. 2693–98.
12. D. Suh, S. Park, T. Lee, C. Oh, and S. Kim: *Metall. Mater. Trans. A*, 2010, vol. 41A, pp. 397–408.
13. H.W. Luo, J. Shi, C. Wang, W.Q. Cao, X.J. Sun, and H. Dong: *Acta Mater.*, 2011, vol. 59, pp. 4002–14.
14. J. Shi, X. Sun, M. Wang, W. Hui, H. Dong, and W. Cao: *Scripta Mater.*, 2010, vol. 63, pp. 815–18.
15. Z.H. Cai, H. Ding, R.D.K. Misra, and Z.Y. Ying: *Acta Mater.*, 2015, vol. 84, pp. 229–36.
16. Q. Han, Y. Zhang and L. Wang: *HMnS2014 conf. Proc.*, Aachen, 2014.
17. S. Lee, S. Lee, and B.C. De Cooman: *Scripta Mater.*, 2011, vol. 64, pp. 649–52.
18. P. J. Gibbs: *Design Consideration for the Third Generation Advanced High Strength Steel*, PhD Thesis, Colorado School of Mines, 2013.
19. J. Hu, L.X. Du, G.S. Sun, H. Xie, and R.D.K. Misra: *Scripta Mater.*, 2015, vol. 104, pp. 87–90.
20. T. Tsuchiyama, T. Inoue, J. Tobata, D. Akama, and S. Takaki: *Scripta Mater.*, 2016, vol. 122, pp. 36–39.
21. Y.K. Lee and J. Han: *Mater. Sci. Technol.*, 2014, vol. 31, pp. 843–56.
22. E. De Moor, D.K. Matlock, J.G. Speer, and M.J. Merwin: *Scripta Mater.*, 2011, vol. 64, pp. 185–88.
23. S. Lee, S. Lee, and B.C. De Cooman: *Int. J. Mate. Res.*, 2013, vol. 104, pp. 423–29.
24. N. Nakada, K. Mizutani, T. Tsuchiyama, and S. Takaki: *Acta Mater.*, 2014, vol. 65, pp. 251–58.
25. A. Kwiatkowski da silva, G. Leyson, M. Kuzmina, D. Ponge, M. Herbig, S. Sandlobes, B. Gault, J. Neugebauer, and D. Raabe: *Acta Mater.*, 2017, vol. 124, pp. 305–15.
26. B.B. He, M.X. Huang, Z.Y. Liang, A.H.W. Ngan, H.W. Luo, J. Shi, W.Q. Cao, and H. Dong: *Scripta Mater.*, 2013, vol. 69, pp. 215–18.
27. S. Lee and B.C. De Cooman: *Metall. Mater. Trans. A*, 2013, vol. 44A, pp. 5018–24.
28. S. Lee, S. Lee, and B.C. De Cooman: *Scripta Mater.*, 2011, vol. 65, pp. 225–28.
29. S. Lee, S. Lee, and B.C. De Cooman: *Acta Mater.*, 2011, vol. 59, pp. 7546–53.
30. R.E. Reed-Hill and R. Abbaschian: *Physics Metallurgy Principles*, M PWS-Kent, Boston, 1992, p. 250.
31. G.B. Olson and M. Cohen: *Metall. Trans. A*, 1975, vol. 6, pp. 791–95.
32. H. Luo, H. Dong, and M. Huang: *Mater. Des.*, 2015, vol. 83, pp. 42–48.
33. X Wang, L Wang, and M Huang: *Mater. Sci. Eng. A*, 2016, vol. 674, pp. 59–63.
34. X.G. Wang, L. Wang, and M.X. Huang: *Acta Mater.*, 2017, vol. 124, pp. 17–29.
35. R. Sarmah and G. Ananthakrishna: *Acta Mater.*, 2015, vol. 91, pp. 192–201.